Clim Dyn (2018) 50:2183–2197
DOI 10.1007/s00382-017-3743-5

Orbital-scale nonlinear response of East Asian summer monsoon to its potential driving forces in the late Quaternary

Liang Yi[1] · **Zhengguo Shi**[2,3] · **Liangcheng Tan**[2] · **Chenglong Deng**[4,5]

Received: 20 December 2016 / Accepted: 26 May 2017 / Published online: 6 June 2017

Abstract We conducted a statistical study to characterize the nonlinear response of the East Asian summer monsoon (EASM) to its potential forcing factors over the last 260 ka on orbital timescales. We find that both variation in solar insolation and global ice volume were responsible for the nonlinear forcing of orbital-scale monsoonal variations, accounting for ~80% of the total variance. Specifically, EASM records with dominated precession variance exhibit a more sensitive response to changes in solar insolation during intervals of enhanced monsoon strength, but are less sensitive during intervals of reduced monsoon strength. In the case of global ice volume with 100-ka variance, this difference is not one of sensitivity but rather a difference in baseline conditions, such as the relative areas of land and sea which affected the land–sea thermal gradient. We therefore suggest that EASM records with dominated precession variance recorded the signal of a shift in the location of the Inter-tropical Convergence Zone, and the associated changes in the incidence of torrential rainfall; while for proxies with dominated 100-ka variance, it recorded changes in the land–sea thermal gradient via its effects on non-torrential precipitation.

Keywords East Asian summer monsoon (EASM) · Nonlinear response · Statistical analysis · Orbital timescale · The late Quaternary

1 Introduction

Within a series of climatic variability, variation on orbital timescales has attracted great attention because of the key role of changes in earth orbital parameters in modulating insolation, and its role in triggering a series of interior interactions in the climate system (Zachos et al. 2001; Ruddiman 2003). Consequently, the study of climatic variability on orbital timescales provides a unique opportunity to study quantitatively the dynamics and mechanism of climatic responses to an unambiguous forcing factor.

As one of six major monsoon systems on the earth (An et al. 2015), the Asian Monsoon plays a critical role in transporting large quantities of heat and moisture to this densely populated region. The transport of heat and moisture has profound implications for socioeconomic systems (Yancheva et al. 2007; Zhang et al. 2008; Cook et al. 2010). Consequently, it has attracted much research attention over the past few decades, ranging from the analysis of climatic proxies in geological achieves to reconstruct monsoonal evolution, to numerical modeling of the monsoon (Wang

Electronic supplementary material The online version of this article (doi:10.1007/s00382-017-3743-5) contains supplementary material, which is available to authorized users.

✉ Liang Yi
yi.liang82@gmail.com; yiliang@tongji.edu.cn

✉ Chenglong Deng
cldeng@mail.iggcas.ac.cn

[1] State Key Laboratory of Marine Geology, Tongji University, Siping Road 1239#, Shanghai 200092, China

[2] State Key Laboratory of Loess and Quaternary Geology, Institute of Earth Environment, Chinese Academy of Sciences, Xi'an 710061, China

[3] CAS Center for Excellence in Tibetan Plateau Earth Sciences, Beijing 100101, China

[4] State Key Laboratory of Lithospheric Evolution, Institute of Geology and Geophysics, Chinese Academy of Sciences, 19# Bei-Tu-Cheng-Xi-Lu, Beijing 100029, China

[5] University of Chinese Academy of Sciences, Beijing 100049, China

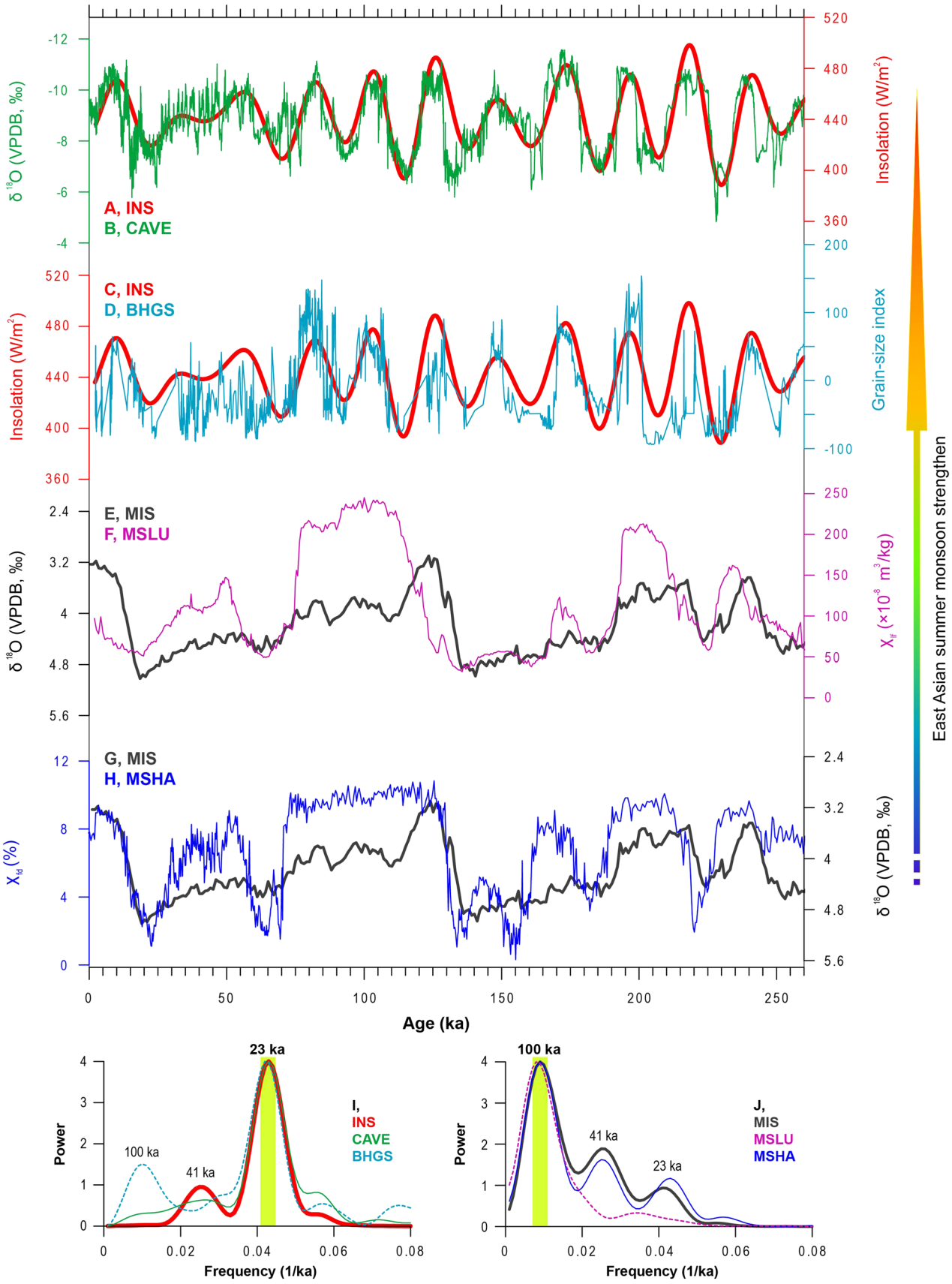
δ18O (VPDB, ‰)
A, INS
B, CAVE
Insolation (W/m2)
C, INS
D, BHGS
Grain-size index
E, MIS
F, MSLU
χlf (×10-8 m3/kg)
G, MIS
H, MSHA
χfd (%)
δ18O (VPDB, ‰)
East Asian summer monsoon strengthen
Age (ka)
23 ka
100 ka
41 ka
I,
INS
CAVE
BHGS
Power
Frequency (1/ka)
100 ka
41 ka
23 ka
J,
MIS
MSLU
MSHA
Power
Frequency (1/ka)

◂**Fig. 1** EASM proxies and their forcing factors. **a, c** 21 July insolation at 65ºN (INS, Berger and Loutre 1991). **b** Stalagmite $\delta^{18}O$ series (CAVE, Cheng et al. 2016). **d** Sediment grain-size record from the Bohai Sea (BHGS, Yi et al. 2012). **e, g** Deep-sea sediment $\delta^{18}O$ records (MIS, Lisiecki and Raymo 2005). **f, h** Magnetic susceptibility record of the Luochuan (MSLU, low frequency data, Lu and An 1997) and Yimaguan profiles (MSHA, frequency-dependent data, Hao et al. 2012), respectively, from the loess–paleosol sequence of the Chinese loess plateau. **i**, **j** Spectral comparison between each paired dataset, following the Blackman–Tukey method (Howell et al. 2006) implemented with the ARAND software package

2006; Wang et al. 2014; An et al. 2015). The geological records investigated include loess deposits (Porter and An 1995; Ding et al. 1995; An et al. 1990, 2001; Guo et al. 2002; Hao et al. 2012; Lu et al. 2013), speleothems (Wang et al. 2001, 2005, 2008a; Cheng et al. 2009, 2016), and marine and lacustrine sediments (Wang et al. 2000; Tian et al. 2008; An et al. 2011; Chen et al. 2015).

Although our understanding of past monsoonal behavior has been enormously increased by these works, the nature of monsoonal variability on orbital timescales and the mechanisms responsible are still hotly debated. So far, the most commonly invoked explanations can be summarized in the form of two scenarios, especially in the case of the East Asian summer monsoon (EASM).

In one scenario, it claims that the EASM is directly controlled by the solar insolation (an external forcing mechanism) (Ruddiman and Raymo 2003; Cheng et al. 2016). According to this viewpoint, the monsoon is interpreted as reflecting the significant displacement of the inter-tropical convergence zone (ITCZ), and that the existence of ITCZ is not dependent upon land–sea thermal contrasts which only provide a favorable longitudinal location for the ITCZ (Wang 1994; Chao and Chen 2001). One of the most significant characteristics of this scenario is that the EASM variability is dominated by precessional cycles, i.e. 19–23 ka, and it is mainly supported by evidence from speleothem records (e.g. Wang et al. 2001; Cheng et al. 2009; Jo et al. 2014).

The other scenario highlights the role of variations in global ice volume in modulating the thermodynamic contrast between the Asian continent and the Pacific Ocean (an internal forcing mechanism) (An et al. 1990), and in this case EASM variability is dominated by the 100 ka eccentricity cycle. There is much evidence to support this latter viewpoint, such as the paleoclimatic records from the deposits of the Chinese Loess Plateau (Porter and An 1995; Ding et al. 1995; An et al. 1990, 2001; Guo et al. 2002; Hao et al. 2012), and from deep-see sediments collected from the South China Sea (Wang et al. 2000; Tian et al. 2008). Previous studies have provided three possible linkages between the EASM and global ice volume: (1) Global sea levels and relative surface areas between the continents and the ocean were changed by global ice volume, and during a glacial stage the increased continental surface area can weaken the transport of heat and moisture (Wang 1999). (2) Increased global ice volume reduces global temperature, while reduce evaporation and thus decrease atmospheric moisture transport (Guo et al. 2002). (3) The Siberian–Mongolian Highs may be strengthened by an extended Arctic ice sheet, thereby enhancing the winter monsoon and reducing the amount of heat and moisture transported from the oceans to land (Ding et al. 1994, 1995).

However, the aforementioned scenarios fail to provide a complete explanation for several key features of the EASM reconstructed from geological evidences. For instance, while the oxygen isotope records of speleothems in China is in phase with August insolation, it does lag June and July insolation by 2–3 ka (Cheng et al. 2016). This is inconsistent with an assumed rapid response of the EASM to insolation. The role of latent heat transport from the Southern Ocean (Clemens et al. 1996, 2008) or heterodyne effects (Clemens et al. 2010; Thomas et al. 2016) might provide an explanation; however, the suggested physical linkages between various climatic systems or processes has not yet been confirmed in the EASM domain.

One possibility for the incomplete level of explanation provided by the two scenarios is that the EASM is controlled by both internal and external factors (Wang 2009), and its response to the forcing factors is a nonlinear process. On this basis, the climatic response to forcing would be more complex than a simple linear model (Ruddiman 2008). In other words, the behavior of the EASM results fundamentally from the complex behavior of the atmosphere and ocean, but the nonlinear mechanisms responsible have not yet been determined. Because of the complexity of the nonlinear system and a wealth of information of the nonlinearity, we focused on testing the possible nonlinear response of the EASM to its forcing factors in this study, by applying several simple statistical methods to the analysis of various EASM proxies and the potential forcing factors on orbital timescales.

2 Studied datasets

There was a significant land–sea transition occurred in East Asia around 0.3 Ma (Yi et al. 2014, 2016), where the total area of these terrestrial basins was >460,000 km^2 (Yi et al. 2015), roughly twice as large as the Great Lakes of North America. The loss of the fresh water and sediments and the presence of the seas inevitably affected environmental processes in East Asia (Yi et al. 2015), but the influence of this transition has not been well assessed yet. Considering the land–sea transition, the ready availability of well-dated proxy records, and the interpretation of which is relatively unambiguous, we selected

the late Quaternary (0–260 ka) for study. Two categories of data were chosen: (1) those reflecting external forcing and (2) those reflecting internal forcing (Fig. 1):

1. The calculated record of 21 July insolation at 65°N (INS, Berger and Loutre 1991) was used to model the external forcing of the EASM, which has broadly been selected in previous studies of the Asian monsoon (e.g. Ruddiman 2006; Cheng et al. 2009), while insolation at 30°N and 20°N were tested as references, since those were also previously mentioned (e.g. Wang et al. 2001; Wang 2009). Stalagmite $\delta^{18}O$ records (CAVE, Cheng et al. 2016), and sediment grain-size record from the Bohai Sea (BHGS, Yi et al. 2012) were used as precession-dominated responses.
2. The $\delta^{18}O$ record from deep-sea sediments (MIS, Lisiecki and Raymo 2005) was selected to represent an internal forcing mechanism. Magnetic susceptibility records from the loess–paleosol sequences at Luochuan (MSLU, low-frequency data, Lu and An 1997) and Yimaguan (MSHA, frequency-dependent data, Hao et al. 2012), from the Chinese loess plateau, were selected to represent a 100 ka-dominated response.

The speleothem records (CAVE) have a robust chronology based on high-precise ^{230}Th dating (Wang et al. 2001, 2008a; Cheng et al. 2009). The grain-size record from the Bohai Sea (BHGS) was obtained from a sediment core located at 37°09′N, 118°58′E, and the variance was summarized using principle component analysis (Yi et al. 2012). The chronology for the BHGS was obtained by tuning to the 21 July insolation at 65°N (INS) together with radiocarbon and luminescence dating (Yi et al. 2012) and was also constrained by magnetostratigraphic analysis (Yi et al. 2015, 2016). The CAVE and BHGS time series are both dominated by precession (23 ka) variance, which comprises ~80% of the total (Fig. 1i). The chronology of the MSLU was obtained by tuning to the SPECMAP record (Lu and An 1997), and that for the MSHA by correlating to the MIS (Hao et al. 2012). The MSLU and MSHA time series are both dominated by a 100-ka component, which also comprises ~80% of the total variance (Fig. 1j). Previous studies of the four time series have verified that they are indicators of the EASM in either the precessional or 100-ka domain (Lu and An 1997; Wang et al. 2001, 2008a; Cheng et al. 2009; Yi et al. 2012; Hao et al. 2012).

3 Statistical tests

3.1 Probability density function (PDF)

The distribution of values in each record was summarized using a probability density function (PDF). The INS exhibits a unimodal Gaussian distribution (Fig. 2a), demonstrating that over the last 260 ka it changed gradually and is internally homogenous.

For the proxy records with dominated precession variance, both CAVE and BHGS exhibit a bimodal Gaussian distribution (Fig. 2b, c), indicating the presence of at least two potential subpopulations within the data. Partitioning the data distribution reveals that the relative percentages of the two subpopulations are similar: 46:54 for the CAVE and 44:56 for the BHGS (Fig. 2b, c).

For proxies with dominated 100-ka variance, the MIS, MSLU and MSHA all exhibit bimodal Gaussian distribution (Fig. 2d–f), indicating the presence of at least two potential subpopulations within the data. The relative percentages of the two subpopulaitons vary between the datasets: 37:63 for the MIS, 27:73 for the MSLU, and 44:56 for the MSHA.

3.2 Correlation

The correlation coefficients among proxy records and forcing factors within each paired dataset were calculated using the bootstrap resampling method, which provides the opportunity to examine the structure of the correlation relationship in detail. The sample size of each resampling was 200 (50 for the one with a total size less than 1000). The total resampling performance was 2000, which provides a significance level of $p < 0.05$ to enable a conservative evaluation of the statistical significance of the correlation.

The results are illustrated in Fig. 3. All of the PDFs of correlation coefficients are asymmetrical. Further mathematical partitioning of the PDFs indicates that two subpopulations can be identified (r1 and r2 in Fig. 3). A correlation matrix (Supplementary Tables S1–2) shows that all of the Pearson correlation coefficients, except for the one between the BHGS and MSLU, are significant at the level $p < 0.05$, and the character of the partial correlation coefficients is similar. In additional, all of the confidence regions, plotted as ellipses in Table S1–2, tend to be round.

3.3 Regression

Regression analysis of each paired dataset was conducted. The results (Supplementary Tables S3–4) indicate that 54 and 34% variance of the CAVE and BHGS, respectively, can be explained by the linear variation in the INS, and 22 and 52% variance of the MSLU and MSHA in the MIS, respectively.

Because only up to 50% variance of the EASM can be explained in a common regression analysis, including 11 types of curve estimation (Supplementary Table S3), a

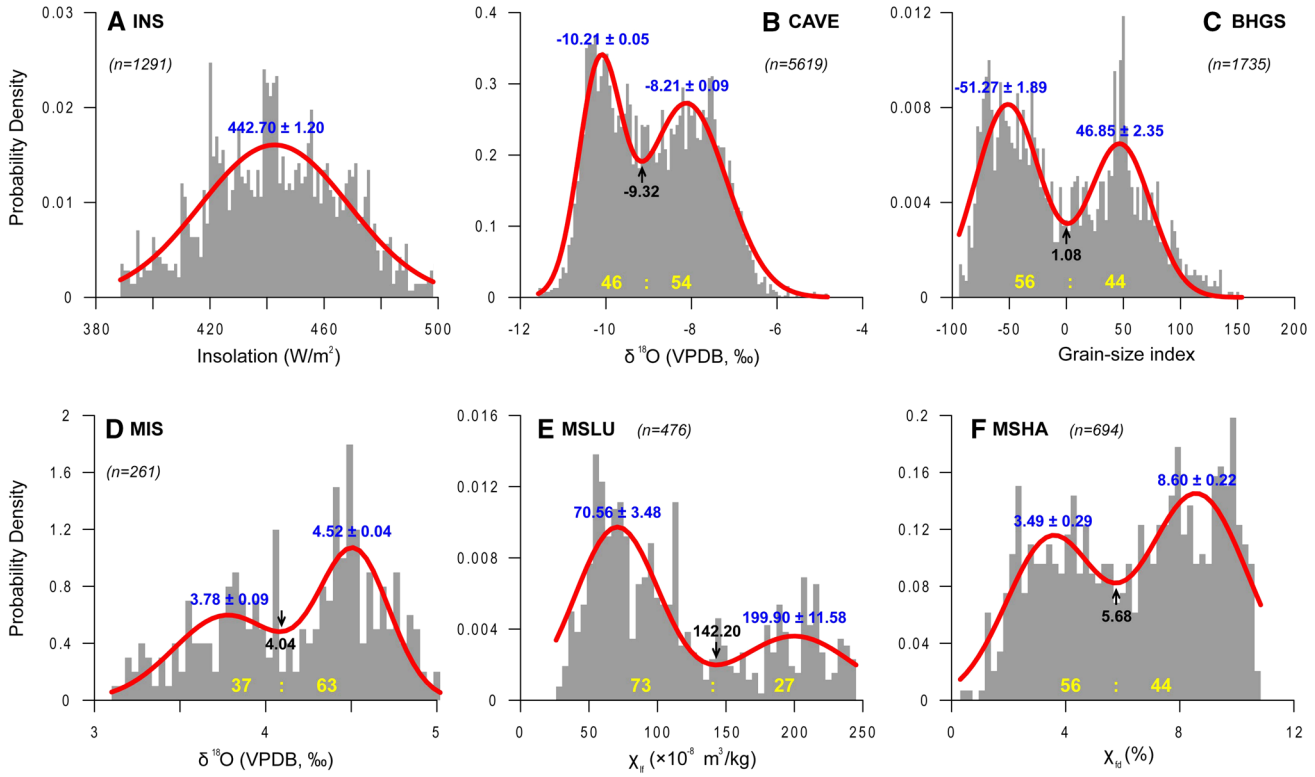

Fig. 2 Probability density function (PDF) of various EASM proxies and their deriving forces. **a** INS (Berger and Loutre 1991); **b** CAVE (Cheng et al. 2016); **c** BHGS (Yi et al. 2012); **d** MIS (Lisiecki and Raymo 2005); **e** MSLU (Lu and An 1997); and **f** MSHA (Hao et al. 2012). The PDF of each series is modeled using a Gaussian distribution. Sample size (n), mean value and relative percentage are also labeled, and the labeled boundary values will be used in latter regression analysis as a dummy variable

nonlinear analysis was conducted. To save the degrees of freedom of the regression, and because two subpopulations were identified in the above analyses in all of the paired datasets (Figs. 2, 3), we simply divide each dataset into two subpopulations according its value changes (Fig. 2). We then conducted regression analysis on each pair of variables by introducing a dummy variable (see details of the dummy variable in Kleinbaum et al. 1997) to preserve the degrees of freedom and general information for the entire dataset. The dummy variable is set according to the data category after subdivision, either 0 or 1. The results are plotted in Fig. 4 and listed in Table S4.

In general, the designed nonlinear regression resulted in a remarkable increase in the explained variance, from 30 to 50% for the linear regression to ~80%. All of the results are significant at the level $p < 0.01$ and they demonstrate the robustness of nonlinear regression for describing the relationship between the EASM and its forcing factors. In the case of CAVE and BHGS, there is no difference between the intercepts but a difference between the slopes; and in contrary, for the MSLU and MSHA, there no difference between the slopes but a difference between the intercepts.

We attempted including the MIS as a variable for the nonlinear regression analysis for the proxy records with dominated precession variance, and the INS as a variable for proxies with dominated 100-ka variance, however, neither was significant. In additional, summer insolation at different latitudes, such as for 21 July insolation at 30°N and 20°N (Berger and Loutre 1991) was further tested, but no essential difference was observed (Supplementary Table S5). Consequently, because none of the nonlinear relationship have the global optima in statistics, we chose this nonlinear regression as a locally optimal solution for latter discussion.

4 Discussion

4.1 Interpretation of statistical observations

All of the statistical tests indicate a significant difference between the forcing factors and the climatic responses. For the records with dominated precession variance, only one peak occurs in the PDF of the INS, but two peaks are evident for both CAVE and BHGS; while for the records with

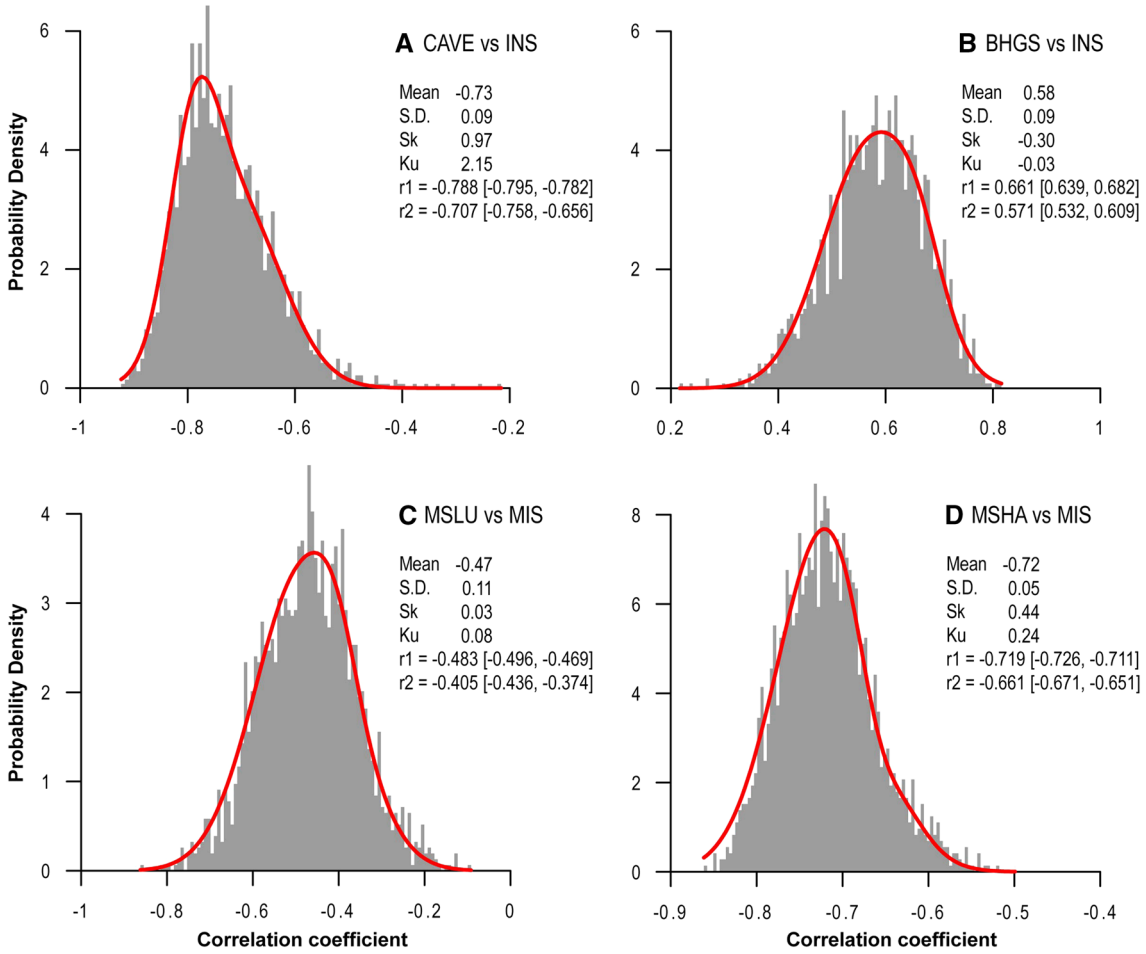

Fig. 3 The results of correlation analysis of EASM proxies and their forcing factors. *Red curves* are the probability density curves fitted with a Gaussian distribution. Statistical parameters for the correlation coefficients are labeled. r1 and r2 are two expectations of subpopulations with a 95% confidence interval. The ranges of the correlation coefficients (*shadow areas*) generally do not cross the origin point, demonstrating their statistical significances

dominated 100-ka variance, the relative percentages of the subpopulations are different in all three records. This phenomenon raises important questions regarding the nature of the internal processes responsible: for the proxy records with dominated precession variance, for generating a climatic response characterized by a bimodal distribution to a forcing function characterized by a unimodal distribution; and for proxies with dominated 100-ka variance, for generating the different relative percentages.

There are two potential explanations for this observation: (*e.1*) Several other factors in addition to the INS or MIS are responsible for driving the EASM; and (*e.2*) more than one type of response process in the EASM is involved during different climatic states, resulting in the observed nonlinearity. Since we lack the evidence to determine which additional factors are responsible for driving the EASM, and since in previous studies typically only a single dominant factor has been considered in the case of both precessional and 100-ka dominances (Wang et al. 2001; Clemens et al. 2008; Wang 2009; Guo et al. 2012), we prefer to regard *e.2* as the most likely explanation.

The results of the correlation and regression analyses clearly demonstrate the nonlinearity of the ESAM to forcing: (1) two relationships within each paired dataset are both significant (Figs. 3, 4); and (2) a potential monsoonal forcing is nonlinearity in general (Fig. 4).

In the regression analysis results for the proxy records with dominated precession variance (Fig. 4a, b), although there is no difference between the intercepts, there is a difference between the slopes. The same intercept coefficient in the regressions indicates that either the origin of the EASM response to solar insolation is the same during different climatic states, or that the basic background driving monsoonal variations for the proxy records with dominated precession variance would not change significantly. On the other hand, a difference in slope indicates that the EASM exhibited different sensitivities (or physical property) to

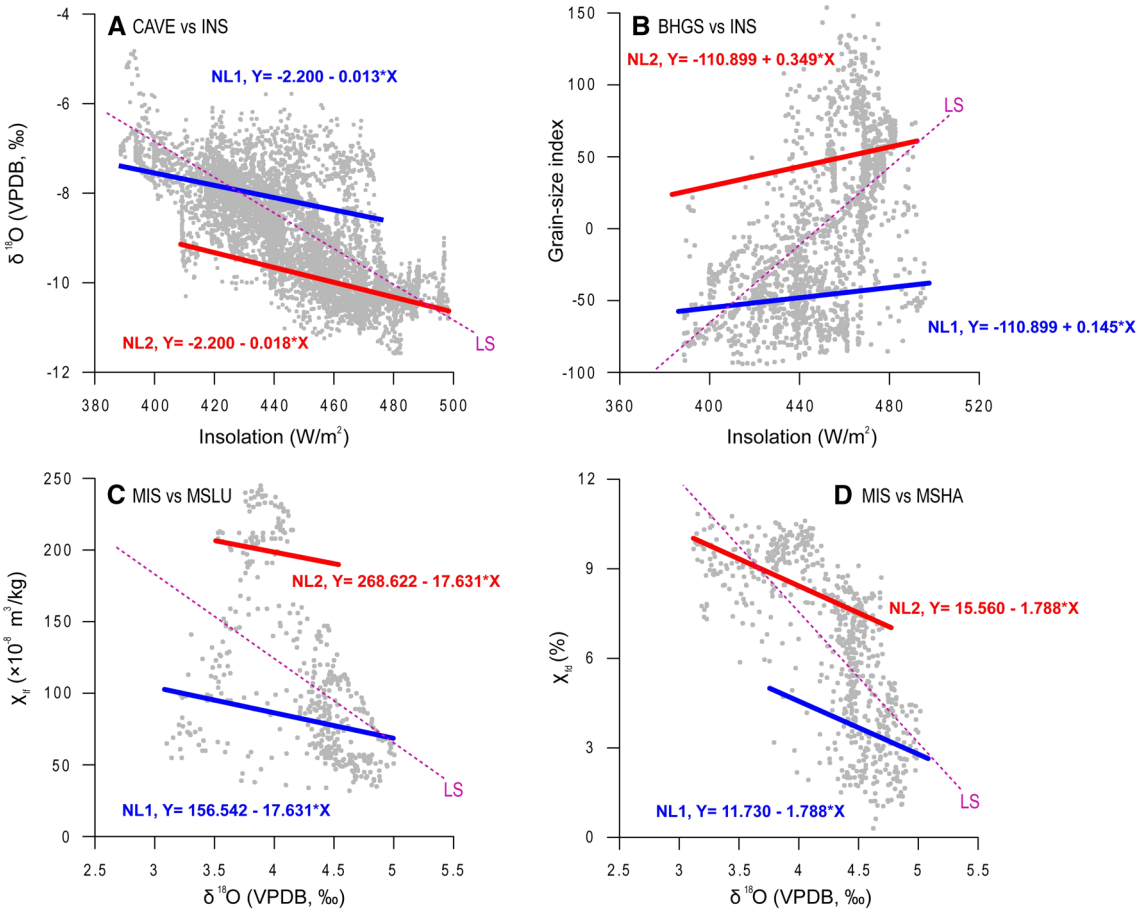

Fig. 4 Results of regression analysis of EASM proxies and their forcing factors. *LS* linear regression as reference, *NL1 and NL2* two equations produced in a nonlinear regression with a dummy variable. See the text and Table S4 for details

forcing in different time intervals. During an interval of enhanced monsoon intensity, the EASM will be more sensitive to changes in insolation, but less sensitive during an interval of reduced intensity.

However, the situation is different in the case of the dominated 100-ka variance (Fig. 4c, d). In this case, there is no difference between the slopes but between the intercepts. This indicates that EASM variability for proxies with dominated 100-ka variance exhibited the same sensitivity to global ice volume changes in both glacial and interglacial stages, but that the baseline conditions varied between different time intervals.

4.2 Possible forcing mechanism

4.2.1 The precessional variance

Relating to the onset of the Asian monsoon in the western Pacific, there is an abrupt shift in the location of the ITCZ in summer from ~7°N to >10° further north (Gray 1968). This meridional migration of the ITCZ has a significant effect on the atmospheric circulations (Chao and Chen 1999), and triggers the onset of monsoon (Chao 2000), independent of any land–sea thermal contrast between the Asian continent and the Pacific Ocean (Wang 1994; Chao and Chen 2001). As a result of its location, this region receives a large daily amount of solar insolation, causing the energy associated with the evaporating water to be converted into sensible heat and generating the ITCZ rain belt with a rain rate of >4 mm/day (Wang 2006).

On orbital timescales, the high-precision ^{230}Th-dated speleothem oxygen isotope records from Hulu, Dongge and Sanbao Caves in China exhibit a dominant and clearly resolved precessional cyclicity (Wang et al. 2001, 2005, 2008a). These stalagmite records reflect variation in the $\delta^{18}O$ of local meteoric precipitation and therefore they can be used to characterize intensity of the EASM (Yuan et al. 2004; Dykoski et al. 2005). This evidence leads to the idea that the EASM can be directly driven by solar insolation (Kutzbach 1981) via the shift in the

location of the ITCZ (Wang et al. 2005; Cheng et al. 2009; Lu et al. 2013; Jo et al. 2014).

The spatial distribution of both annual and summer rainfall across mainland China exhibits a more precisely meridional effect, descending from low to high latitudes (Fig. 5a, b). This meridional distribution of rainfall supports the conclusion from the $\delta^{18}O$ studies of speleothems in China, regarding the location of the ITCZ in summer. However, it cannot explain the occurrence of two monsoonal records at latitudes >37°N, both of which exhibit a strong precessional component (Yi et al. 2012; Jo et al. 2014). Notably, both records are located northwards of two paleoclimatic records from 35 to 36°N which exhibit strong 100-ka variance (Lu and An 1997; Hao et al. 2012).

Although the similar degree of heating of the air masses over Siberian and the northwest Pacific might cancel out the 100-ka signal from paleoclimatic records, resulting in the dominance of 23-ka cyclicity (Nakagawa et al. 2008), one significant issue needs to be addressed. That is the EASM records with dominated precession variance responds more sensitively to changes in solar insolation during an interval of enhanced monsoon intensity (Fig. 4a,

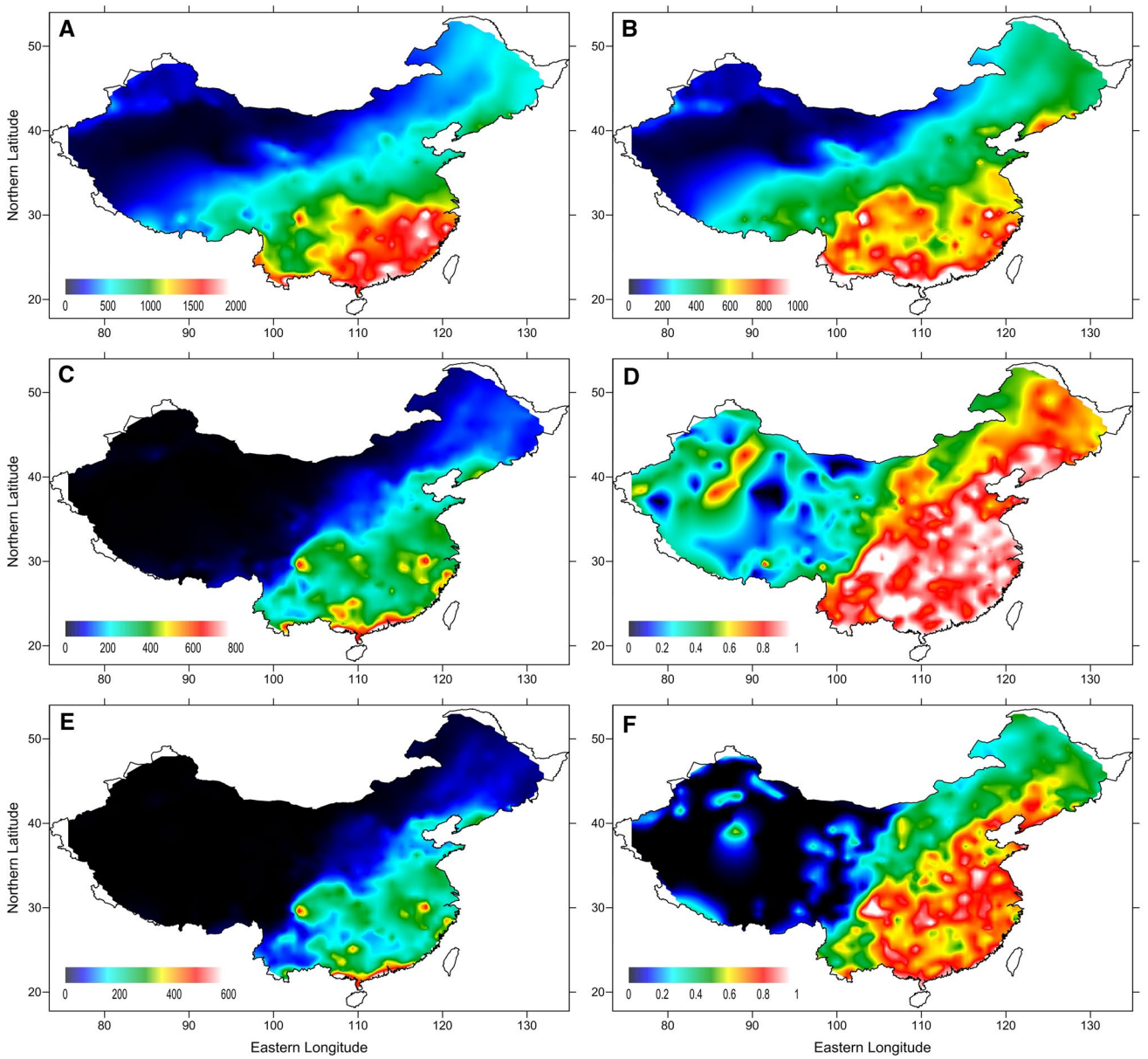

Fig. 5 Distribution of torrential rainfall over mainland China. **a** Annual rainfall (mm), **b** summer (JJAS) rainfall (mm), **c, e** torrential rainfall in summer (mm), ≥30 and 50 mm/day, respectively; **d, f** variance ratio of torrential rainfall and total summer rainfall. Daily rainfall data (1951–2004) are from the China Meteorological Administration (http://data.cma.cn)

b). According to the Antoine equation $\left[\log_{10}(p) = A - \frac{B}{C+T}\right]$ in thermodynamics, in which p is the vapor pressure, T is temperature, A, B and C are constants, for a specific liquid, high temperature leads to high evaporation within the ITCZ zone, and there should be no threshold which changes the nature of the evaporation process. This indicates that some key climatic linkages are undefined.

On the other hand, the summertime location of the ITCZ is also a favorable area for tropical cyclogenesis (Briegel and Frank 1997), and at times when the genesis of tropical cyclone in the western Pacific is frequent, the average amount of summer rainfall increases significantly in Northeast Asia (Choi and Moon 2015; Choi et al. 2016). It has been argued that the correlation between sea surface temperature (SST) and tropical cyclogenesis is insignificant from a observational perspective (Chan and Liu 2004). However, a positive relationship between SST or global warming and tropical cyclogenesis (Webster et al. 2005; Emanuel 2005; Wada and Usui 2007; Tu et al. 2009; Huang et al. 2015; Mei et al. 2015), and between typhoon activity and monsoon intensity (Ren et al. 2002; Kumar and Krishnan 2005; Chang et al. 2012; Holbach and Bourassa 2014; Choi et al. 2016), is broadly claimed based on observations and numerical modeling. In this case, the possibility of tropical cyclogenesis significantly increase since local SSTs are higher than 26–27 °C, while below this temperature threshold, tropical cyclogenesis decreases abruptly to a much low level (Gray 1968; Whitney and Hobgood 1997; Wada and Usui 2007).

It is estimated that the average rainfall associated with typhoons across mainland China during 1951–2004 AD exceeded 700 mm/year (Wang et al. 2008b). Considering the average number of typhoons influencing mainland China, the rainfall intensity associated with these precipitation events can be regarded as near-torrential. Although not all torrential rainfall events are related to typhoon activities, they do be significantly positively correlated with typhoons (Yue et al. 2000; Ren et al. 2002; Jian and Yu 2006; Yao et al. 2009; Sun et al. 2010; Shen et al. 2013). Accordingly, we used the definition of torrential rainfall by the China Meteorological Administration, and removed all data with <30 and <50 mm/day to produce two datasets which were used to detect the spatial distribution of torrential rainfall and their ratios with total summer rainfall across mainland China (Fig. 5).

Unlike the spatial distribution of annual and summer rainfalls (Fig. 5a, b), the distribution of torrential rainfall exhibits a SE–NW descending trend (Fig. 5c, e). The contribution of torrential rainfall to summer rainfall is not very high (Wang et al. 2008b), but it does account for >70% of the variance of summer rainfall (Fig. 5d, f). Moreover, unlike annual and summer rainfall, which gradually descends from low to high latitudes (Fig. 5a, b), torrential rainfall exhibits a clear, narrow boundary at the ratio of ~0.6 (Fig. 5d, f). It implies that the factor controlling the occurrence of torrential rainfall has a distinct spatial limit, and this limit matches well with the spatial influence of typhoon during the past several decades (e.g. Sun et al. 2010; Mendelsohn et al. 2012; Shen et al. 2013) (Supplementary Figure S1). Based on these lines of evidence, we propose that the ITCZ and associated tropical cyclogensis played a crucial role in generating the precessional records of ESAM variability on an orbital timescale.

4.2.2 The 100-ka variance

It has been long identified that the existence of continental-scale land–sea thermal contrast is the main factor responsible for monsoon circulation (Wallace and Hobb 1977; Webster et al. 1998; Wang and Ding 2008). In summer, radiative heating produces a thermal low in the continent and a relative high over the ocean, resulting in the inflow of low-level winds over the continent, and creating a moisture convergence. In winter, radiative cooling of the continent results in a thermal high and, to its southeast, low-level winds flow northeastward.

According to the results of atmospheric monitoring and numerical modeling, monsoonal precipitation across mainland China is mainly derived from the Arabian Sea, Indian Ocean and South China Sea (Ding and Chan 2005; Ding and Sikka 2006; Pausata et al. 2011; Liu et al. 2014). Hence, in principle summer rainfall should decrease in the direction of moisture transport, however, we do not observe this trend in the spatial distribution of summer rainfall across mainland China (Fig. 6a, b). Considering the aforementioned contribution of summer rainfall from tropical cyclones, we remove all rainfall events with intensity ≥30 and ≥50 mm/day in order to portray the spatial distribution of non-torrential summer rainfall and the ratios of average summer rainfall to total summer rainfall across mainland China (Fig. 6).

Unlike the spatial distribution of annual and summer rainfalls (Fig. 6a, b), the distribution of average rainfall exhibits a descending trend from the coast to inland (Fig. 6c, e), consistent with the transport of monsoonal moisture. Moreover, it accounts for >80% of the variance of summer rainfall within the inland China, including the main part of the Chinese Loess Plateau (Fig. 6d, f). Consequently, this implies that summer rainfall associated with land–sea thermal contrast can be characterized as normal, non-torrential rainfall across mainland China.

On orbital timescales, EASM variability recorded in aeolian deposits from the Chinese Loess Plateau is dominated by the 100-ka cyclicity (Lu and An 1997; Hao et al. 2012), as is also reported for deep-see sediments from

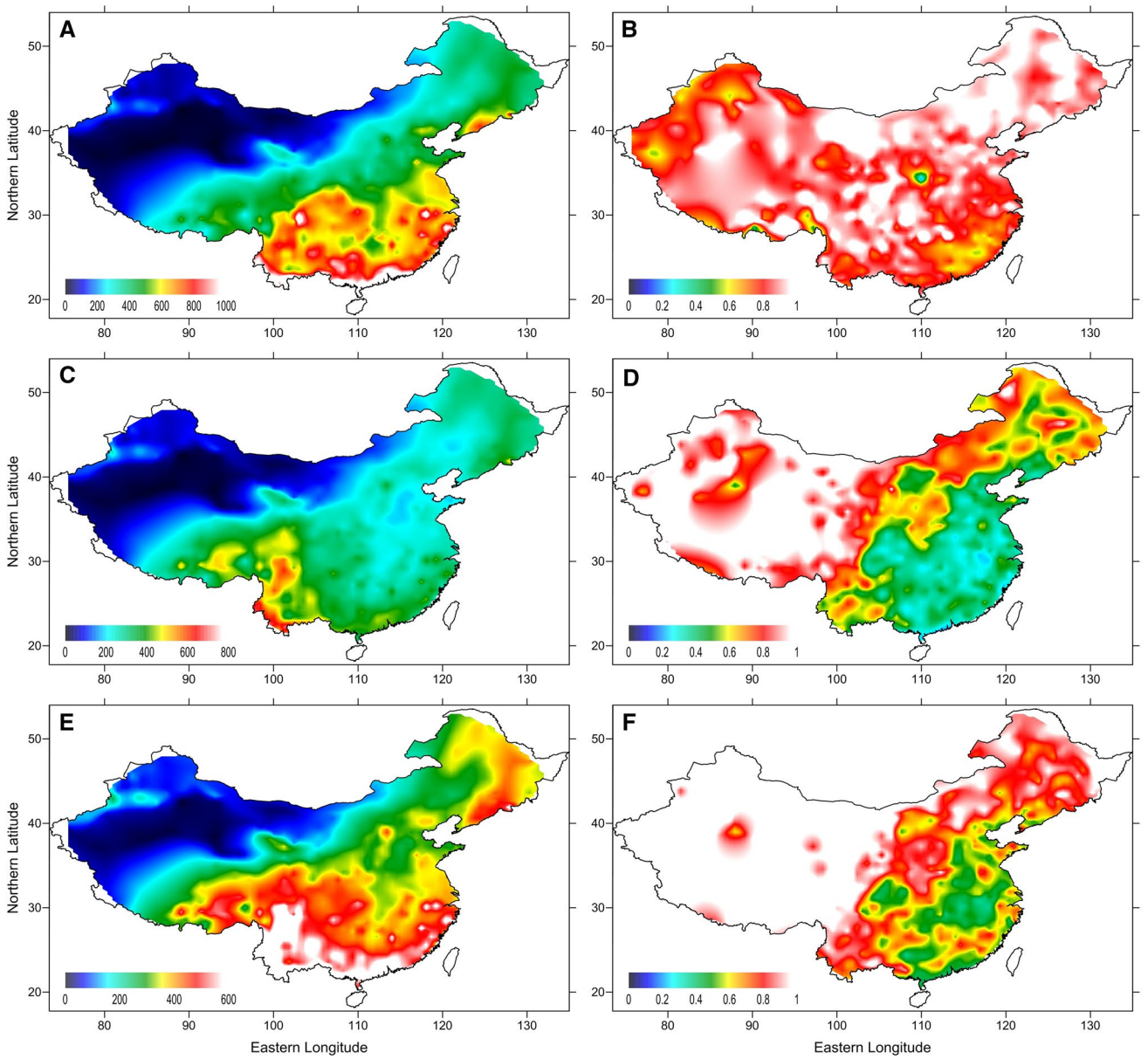

Fig. 6 Distribution of non-torrential precipitation over mainland China. **a, b** Summer (JJAS) rainfall (mm) and its ratio to the annual value; **c, e** non-torrential rainfall in summer (mm), <30 and <50 mm/day, respectively; **d, f** variance ratio of non-torrential rainfalls. Daily data (1951–2004 AD) are from the China Meteorological Administration (http://data.cma.cn)

the South China Sea (Wang et al. 2000; Tian et al. 2008). The magnetic susceptibility record of the loess–palaeosol sequence of the Chinese Loess Plateau, which reflects the pedogenic production of secondary ferrimagnetic minerals, is regarded as a reliable proxy for the EASM intensity (An et al. 1990; Ding et al. 1995; Porter and An 1995; Sun et al. 2006; Yang et al. 2015). This record has been used to propose the major role of variations in global ice volume in modulating the thermodynamics of land–sea contrast (An et al. 1990).

Although several possible linkages between EASM variability and global ice volume have been proposed (An et al. 1990; Ding et al. 1994, 1995; Wang 1999; Guo et al. 2002), our regression results indicate that the same sensitivity but distinct difference in baseline conditions during different climatic states (Fig. 4c, d). This difference in baseline conditions may conceivably relate to changes in the relative areas of land and sea between glacial and interglacial intervals. For example, it has been proposed that the ratio of the areas of land and sea in South Asia could decrease

from 1:1.6 to 1:4.1 during interglacials (De Decker et al. 2002). This estimate may be applicable to East Asia, given the very shallow slope of the continental shelf areas. Hence, we propose that global ice volume and associated land–sea changes played a crucial role in generating the 100-ka cyclicity in ESAM variability on orbital timescales.

4.2.3 Linkages between EASM proxies and driving factors

The summer atmospheric circulation across the Asia continent and northwest Pacific Ocean exhibits a pattern of wind flow from the Indian Ocean to mainland China. Moreover, winds from the western Pacific only reach East China (Fig. 7a), supporting the idea that almost all the monsoonal moisture is derived from the Arabian Sea, Indian Ocean and South China Sea (Ding and Chan 2005; Ding and Sikka 2006), especially in the case of non-torrential rainfall. However, this circulation pattern will be disrupted during the formation and movement of typhoons. For instance, during Typhoon Chan-hom (Fig. 7b), southeasterly winds penetrated into mainland China on a large scale, extending westwards to 105°E.

The observed difference in atmospheric circulation patterns with and without the occurrence of tropical cyclones supports the hypothesis that rainfall delivered by the EASM has two potential sources: the first consisting of moisture from the Indian Ocean and South China Sea alone; and the second, during intervals with an increased incidence of typhoons, when moisture from the first source is supplemented and renewed by an additional source from the Pacific Ocean. It is possible that variations in the monsoonal proxies in the 100 and 23-ka variances are linked to differences in the contributions from these two sources.

Typically, not all of the precipitation infiltrates into the soil. Some precipitation may be lost to evaporation and surface runoff, and thus the component remaining in the soil is termed effective precipitation. Because of the soil characteristics in the Chinese Loess Plateau, it is likely that only non-torrential precipitation, which probably approximates the effective precipitation, is stored in the soil and becomes available to participate in the biochemical processes responsible for pedogenesis and the production of the secondary ferrimagnetic minerals that dominate the magnetic susceptibility record. Since average precipitation accounts for >80% of the variance of total rainfall in summer (Fig. 6d, f), the magnetic susceptibility signal of the loess–palaeosol sequence probably reflects variations in non-torrential summer precipitation, which is directly correlated with the land–sea thermal contrast (Fig. 6), as mentioned earlier. We suggest that this linkage is responsible for the dominant 100-ka cyclicity of EASM variability on orbital timescales.

Due to the complex processes involved in the penetration of drip water into caves, various linkages between oxygen isotopic changes of speleothems have been proposed, such as that it reflects local rainfall on an annual or decadal scale (e.g. McDermott 2004; Genty et al. 2014), seasonal surface precipitation (e.g. Cruz et al. 2005; Genty 2008), present-day precipitation with stored water (Duan et al. 2016), and torrential rains in the wet season (Bar-Matthews et al. 1996; Jones et al. 2000; Jones and Banner 2003; Pape et al. 2010). Considering the strongly depleted $\delta^{18}O$ values of typhoon rainfalls (e.g. Fudeyasu et al. 2008; Zhang et al. 2009; Sun et al. 2016), we suggest that the $\delta^{18}O$ record of Chinese speleothems within the EASM domain probably supports the conclusion that is reflects torrential rainfall during the wet season. Since tropical cyclogenesis is usually frequent from July to September, typically reaching a maximum in August in the western Pacific (Whitney and Hobgood 1997; Chan 2005; Wang et al. 2007; Stowasser et al. 2007; Wada et al. 2012), this linkage between stalagmite $\delta^{18}O$ changes and torrential rainfall is consistent with the observed in-phase relationship (zero offset) between $\delta^{18}O$ changes and solar insolation in the northern hemisphere in August (e.g. Cheng et al. 2016).

The sediment grain-size record from the Bohai Sea (Yi et al. 2012) further supports this conclusion regarding the significance of changes in the $\delta^{18}O$ of Chinese speleothems. Coarse sedimentary particles can only be mobilized given sufficient energy of the transport medium, and once deposited, they cannot be re-suspended without an increase in that energy. In the Bohai Sea, sediment grain-size variation is controlled by river discharge and re-suspension process in the tidal zone (Yi et al. 2012; Li et al. 2014). Based on the operation of these sedimentary processes (Chen et al. 2013; Su et al. 2016), we suggest that torrential rainfall events played a crucial role in driving the sedimentary grain-size variations observed in the sediments of the Bohai Sea. Therefore, in combination with the character of Chinese stalagmite $\delta^{18}O$ changes, we conclude that this linkage is responsible for the precession-dominated character of EASM variability on orbital timescales.

5 Conclusions

In order to characterize the variation and dynamics of the EASM on orbital timescales, we conduct a study of the relationship between EASM proxies and their forcing mechanisms during the late Quaternary. The most noticeable feature of the EASM proxies is that they exhibit a nonlinear response to their forcing factors. As a result, we

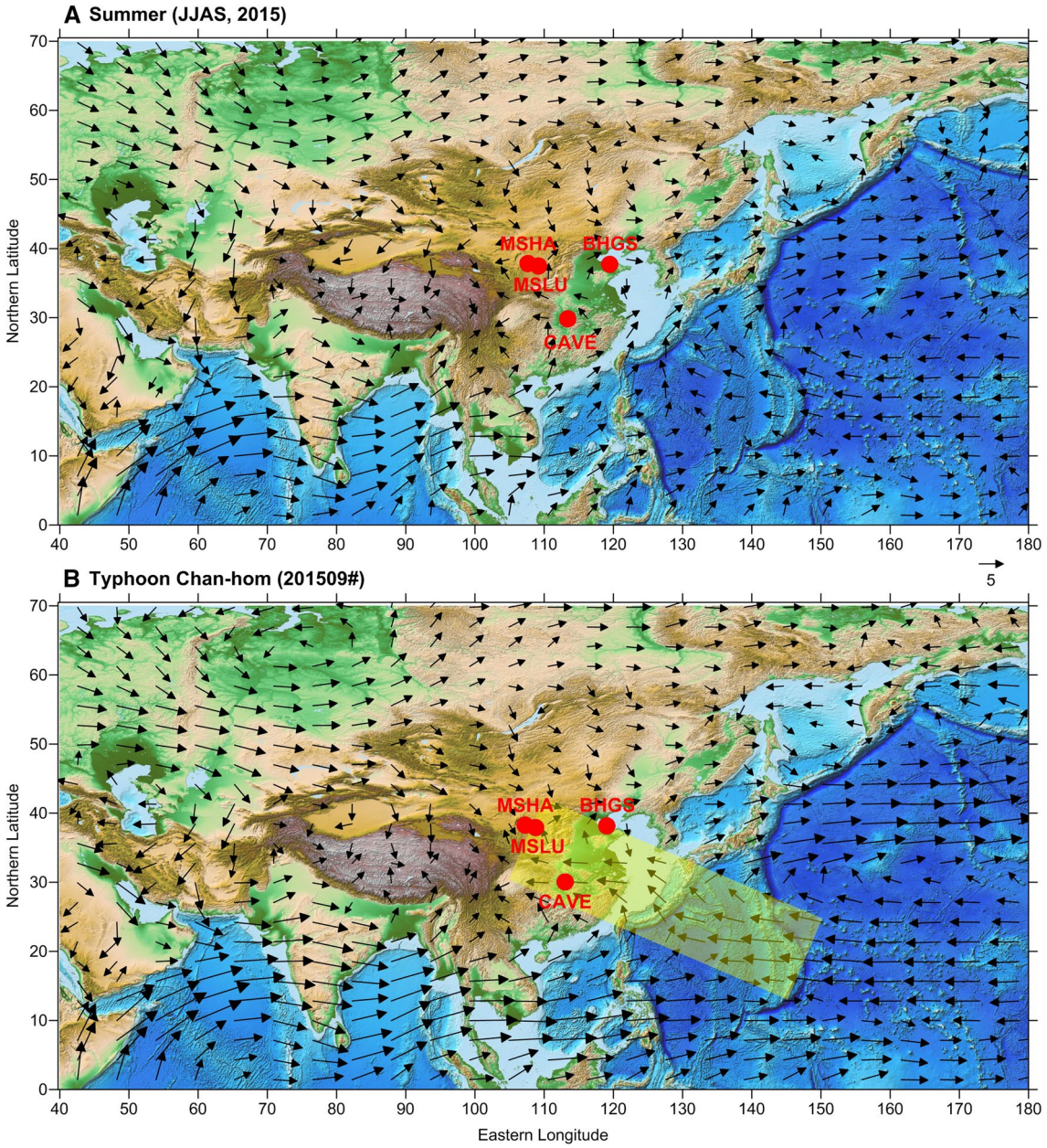

Fig. 7 Atmospheric circulation across the Asia continent and northwest Pacific Ocean. **a** Average summer values from June to September (JJAS), 2015; **b** average values during Typhoon Chan-hom (Namtheun, 201509#) from July 1–10, 2015. The *shaded yellow area* indicates the incursion of Pacific moisture into mainland China during a tropical cyclone. The latitudes of four geological records used in this study are 31.67 N (CAVE), 37.15 N (BHGS), 35.71 N (MSLU), and 35.89 N (MSHA). The origin data for the 850 hPa wind vectors are from the European Centre for Medium-Range Weather Forecasts Reanalysis (ERA) data (Dee et al. 2011) (http://apps.ecmwf.int). The base map data are from http://www.ngdc.noaa.gov/mgg/global/global.html

propose different types of linkage of the EASM proxy to the dominant forcing factors, as follows.

Solar insolation and global ice volume both account for ~80% of the total variance in EASM variability; however, the relationships are nonlinear. Specifically, the EASM records with dominated precession variance was more sensitive to changes in solar insolation during intervals of increased EASM strength, but was less sensitive during intervals of decreased strength. For proxies with dominated 100-ka variance, the difference is not one of sensitivity but rather of a difference in baseline conditions. Combining this finding with an analysis of the spatial distribution of different types of summer rainfall, we conclude that for the proxy records with dominated precession variance, EASM variability was linked to the shift in the ITCZ via torrential rainfall. In contrast, for proxies with dominated 100-ka

variance, it was linked to changes in the land–sea thermal gradient associated with non-torrential rainfall.

However, this study is based solely on statistical analysis of geological records and is only based on a single forcing factor for the EASM proxies and one mathematical equation to express the nonlinear process. In addition, simply splitting the dataset into two subpopulations may introduce uncertainties into the regression analysis. Therefore, we suggest that the use of an increased number of paleoclimatic records with a broader spatial coverage, together with further numerical modeling, are necessary in future research.

Acknowledgements We thank Drs. Junyi Ge, Ying Zhang and Xin Zhou for their discussion of an early version of this manuscript; Profs. Jan Bloemendal, Zhimin Jian and Joseph D Ortiz for their important helps and discussion; and three anonymous reviewers for their suggestion and comments in improving this manuscript. The research was supported by the National Natural Science Foundation of China (NSFC 41690112 and 41402153) and National Programme on Global Change and Air–Sea Interaction of China (GASI-GEOGE-04). L.T. acknowledges further support from the NSFC (41290254). Part of this work was completed while the lead author conducted a post-doc at Institute of Geology and Geophysics, Chinese Academy of Sciences, and Department of Geology, Kent State University.

References

An Z, Liu TS, Lu YC, Porter SC, Kukla G, Wu XH, Hua YM (1990) The long-term palaeomonsoon variation recorded by the loess-paleosol sequence in central China. Quat Int 7/8:91–95

An Z, Kutzbach JE, Prell WL, Porter SC (2001) Evolution of Asian monsoons and phased uplift of the Himalaya-Tibetan plateau since Late Miocene times. Nature 411:62–66

An Z, Clemens SC, Shen J, Qiang X, Jin Z, Sun Y, Prell WL, Luo J, Wang S, Xu H, Cai Y, Zhou W, Liu X, Liu W, Shi Z, Yan L, Xiao X, Chang H, Wu F, Ai L, Lu F (2011) Glacial-interglacial indian summer monsoon dynamics. Science 333:719–723

An Z, Wu G, Li J, Sun Y, Liu Y, Zhou W, Cai Y, Duan A, Li L, Mao J, Cheng H, Shi Z, Tan L, Yan H, Ao H, Chang H, Feng J (2015) Global monsoon dynamics and climate change. Annu Rev Earth Planet Sci 43:29–77

Bar-Matthews M, Ayalon A, Matthews A, Sass E, Halicz L (1996) Carbon and oxygen isotope study of the active water–carbonate system in a karstic Mediterranean cave: Implications for paleoclimate research in semiarid regions. Geochim Cosmochim Acta 60:337–347

Berger A, Loutre MF (1991) Insolation values for the climate of the last 10 million years. Quat Sci Rev 10:297–317

Briegel LM, Frank WM (1997) Large-scale influences on tropical cyclogenesis in the Western North Pacific. Mon Weather Rev 125:1397–1413

Chan JCL (2005) Interannual and interdecadal variations of tropical cyclone activity over the western North Pacific. Meteorol Atmos Phys 89:143–152

Chan JCL, Liu KS (2004) Global warming and Western North Pacific typhoon activity from an observational perspective. J Clim 17:4590–4602

Chang C-P, Lei Y, Sui C-H, Lin X, Ren F (2012) Tropical cyclone and extreme rainfall trends in East Asian summer monsoon since mid-20th century. Geophys Res Lett 39:L18702

Chao WC (2000) Multiple quasi equilibria of the ITCZ and the origin of monsoon onset. J Atmos Sci 57:641–652

Chao WC, Chen B (1999) Approximate co-location of precipitation and low-level westerlies in tropical monthly means. Paper presented at the climate variations, Denver

Chao WC, Chen B (2001) The origin of monsoons. J Atmos Sci 58:3497–3507

Chen G, Yi L, Chen S, Huang H, Liu Y, Xu Y, Cao J (2013) Partitioning of grain-size components of estuarine sediments and implications for sediment transport in southwestern Laizhou Bay, China. Chin J Oceanol Limnol 31:895–906

Chen F, Xu Q, Chen J, Birks HJB, Liu J, Zhang S, Jin L, An C, Telford RJ, Cao X, Wang Z, Zhang X, Selvaraj K, Lu H, Li Y, Zheng Z, Wang H, Zhou A, Dong G, Zhang J, Huang X, Bloemendal J, Rao Z (2015) East Asian summer monsoon precipitation variability since the last deglaciation. Sci Rep 5:11186

Cheng H, Edwards RL, Broecker WS, Denton GH, Kong X, Wang Y, Zhang R, Wang X (2009) Ice age terminations. Science 326:248–252

Cheng H, Edwards RL, Sinha A, Spötl C, Yi L, Chen S, Kelly M, Kathayat G, Wang X, Li X, Kong X, Wang Y, Ning Y, Zhang H (2016) The Asian monsoon over the past 640,000 years and ice age terminations. Nature 534:640–646

Choi K-S, Moon I-J (2015) Connection between the genesis number of tropical cyclones over the western North Pacific and summer rainfall over Northeast Asia. Theor Appl Climatol 122:353–363

Choi K-S, Cha Y, Kim H-D, Kang S-D (2016) Possible relationship between East Asian summer monsoon and western North Pacific tropical cyclone genesis frequency. Theor Appl Climatol 124:81–90

Clemens SC, Murray DW, Prell WL (1996) Nonstationary phase of the plio-pleistocene Asian monsoon. Science 274:943–948

Clemens SC, Prell WL, Sun Y, Liu Z, Chen G (2008) Southern hemisphere forcing of Pliocene $\delta^{18}O$ and the evolution of Indo-Asian monsoons. Paleoceanography 23:PA4210

Clemens SC, Prell WL, Sun Y (2010) Orbital-scale timing and mechanisms driving Late Pleistocene Indo-Asian summer monsoons: Reinterpreting cave speleothem $\delta^{18}O$. Paleoceanography 25:PA4207

Cook ER, Anchukaitis KJ, Buckley BM, D'Arrigo RD, Jacoby GC, Wright WE (2010) Asian monsoon failure and megadrought during the last millennium. Science 328:486–489

Cruz FW Jr, Karmann I, Viana O Jr, Burns SJ, Ferrari JA, Vuille M, Sial AN, Moreira MZ (2005) Stable isotope study of cave percolation waters in subtropical Brazil: Implications for paleoclimate inferences from speleothems. Chem Geol 220:245–262

De Deckker P, Tapper NJ, van der Kaars S (2002) The status of the Indo-Pacific Warm Pool and adjacent land at the Last Glacial Maximum. Global Planet Change 35:25–35

Dee DP, Uppala SM, Simmons AJ, Berrisford P, Poli P, Kobayashi S, Andrae U, Balmaseda MA, Balsamo G, Bauer P, Bechtold P, Beljaars ACM, van de Berg L, Bidlot J, Bormann N, Delsol C, Dragani R, Fuentes M, Geer AJ, Haimberger L, Healy SB, Hersbach H, Hólm EV, Isaksen L, Kållberg P, Köhler M, Matricardi M, McNally AP, Monge-Sanz BM, Morcrette JJ, Park BK, Peubey C, de Rosnay P, Tavolato C, Thépaut JN, Vitart F (2011) The ERA-Interim reanalysis: configuration and performance of the data assimilation system. Q J R Meteorol Soc 137:553–597

Ding Y, Chan LJC (2005) The East Asian summer monsoon: an overview. Meteorol Atmos Phys 89:117–142

Ding Y, Sikka DR (2006) Synoptic systems and weather. In: Wang B (ed) The asian monsoon. Springer Berlin Heidelberg, Berlin, pp 131–201

Ding Z, Yu Z, Rutter NW, Liu TS (1994) Towards an orbital time scale for Chinese loess deposits. Quat Sci Rev 13:39–70

Ding Z, Liu T, Rutter NW, Yu Z, Guo Z, Zhu R (1995) Ice-volume forcing of East Asian winter monsoon variations in the past 800,000 years. Quat Res 44:149–159

Duan W, Ruan J, Luo W, Li T, Tian L, Zeng G, Zhang D, Bai Y, Li J, Tao T, Zhang P, Baker A, Tan M (2016) The transfer of seasonal isotopic variability between precipitation and drip water at eight caves in the monsoon regions of China. Geochim Cosmochim Acta 183:250–266

Dykoski CA, Edwards RL, Cheng H, Yuan D, Cai Y, Zhang M, Lin Y, Qing J, An Z, Revenaugh J (2005) A high-resolution, absolute-dated Holocene and deglacial Asian monsoon record from Dongge Cave, China. Earth Planet Sci Lett 233:71–86

Emanuel K (2005) Increasing destructiveness of tropical cyclones over the past 30 years. Nature 436:686–688

Fudeyasu H, Ichiyanagi K, Sugimoto A, Yoshimura K, Ueta A, Yamanaka MD, Ozawa K (2008) Isotope ratios of precipitation and water vapor observed in Typhoon Shanshan. J Geophys Res 113:D12113

Genty D (2008) Palaeoclimate research in Villars Cave (Dordogne, SW-France). Int J Speleol 37:173–191

Genty D, Labuhn I, Hoffmann G, Danis PA, Mestre O, Bourges F, Wainer K, Massault M, Van Exter S, Régnier E, Orengo P, Falourd S, Minster B (2014) Rainfall and cave water isotopic relationships in two South-France sites. Geochim Cosmochim Acta 131:323–343

Gray WM (1968) Global view of the origin of tropical disturbances and storms. Mon Weather Rev 96:669–700

Guo Z, Ruddiman WF, Hao Q, Wu H, Qiao Y, Zhu R, Peng S, Wei JJ, Yuan B, Liu TS (2002) Onset of Asian desertification by 22 Myr ago inferred from loess deposits in China. Nature 416:159–163

Guo Z, Zhou X, Wu H (2012) Glacial-interglacial water cycle, global monsoon and atmospheric methane changes. Clim Dyn 39:1073–1092

Hao Q, Wang L, Oldfield F, Peng S, Qin L, Song Y, Xu B, Qiao Y, Bloemendal J, Guo Z (2012) Delayed build-up of Arctic ice sheets during 400,000-year minima in insolation variability. Nature 490:393–396

Holbach HM, Bourassa MA (2014) The effects of gap-wind-induced vorticity, the monsoon trough, and the ITCZ on East Pacific tropical cyclogenesis. Mon Weather Rev 142:1312–1325

Howell P, Pisias N, Ballance J, Baughman J, Ochs L (2006) ARAND time-series analysis software. Brown University, Providence

Huang P, Lin II, Chou C, Huang R-H (2015) Change in ocean subsurface environment to suppress tropical cyclone intensification under global warming. Nat Commun 6:7188

Jian J, Yu J (2006) Relationship between landfalling typhoons and summer precipitation over north China. J Nanjing Inst Meteorol 29:819–826

Jo K-N, Woo KS, Yi S, Yang DY, Lim HS, Wang Y, Cheng H, Edwards RL (2014) Mid-latitude interhemispheric hydrologic seesaw over the past 550,000 years. Nature 508:378–382

Jones IC, Banner JL (2003) Estimating recharge thresholds in tropical karst island aquifers: Barbados, Puerto Rico and Guam. J Hydrol 278:131–143

Jones IC, Banner JL, Humphrey JD (2000) Estimating recharge in a tropical Karst Aquifer. Water Resour Res 36:1289–1299

Kleinbaum D, Kupper L, Muller K, Nizam A (1997) Applied regression analysis and other multivariable methods. Duxbury Press, Pacific Grove

Kumar V, Krishnan R (2005) On the association between the Indian summer monsoon and the tropical cyclone activity over northwest Pacific. Curr Sci 88:602–613

Kutzbach JE (1981) Monsoon climate of the early Holocene: climate experiment with the earth's orbital parameters for 9000 years ago. Science 214:59–61

Li Y, Yu H, Yi L, Su Q, Hu K, Xu X, Wang J (2014) Grain-size characteristics and its sedimentary significance of coastal sediments of the borehole Lz908 in the south Bohai Sea (the Laizhou Bay), China. Mar Sci 38:107–113

Lisiecki LE, Raymo ME (2005) A Pliocene-Pleistocene stack of 57 globally distributed benthic $\delta^{18}O$ records. Paleoceanography 20:PA1003

Liu Z, Wen X, Brady EC, Otto-Bliesner B, Yu G, Lu H, Cheng H, Wang Y, Zheng W, Ding Y, Edwards RL, Cheng J, Liu W, Yang H (2014) Chinese cave records and the East Asia Summer Monsoon. Quat Sci Rev 83:115–128

Lu H, An Z (1997) Paleoclimatic significance of grain size composite of loess deposit in Luochuan. Chin Sci Bull 42:66–69

Lu H, Yi S, Liu Z, Mason JA, Jiang D, Cheng J, Stevens T, Xu Z, Zhang E, Jin L, Zhang Z, Guo Z, Wang Y, Otto-Bliesner B (2013) Variation of East Asian monsoon precipitation during the past 21 k.y. and potential CO_2 forcing. Geology 41:1023–1026

McDermott F (2004) Palaeo-climate reconstruction from stable isotope variations in speleothems: a review. Quat Sci Rev 23:901–918

Mei W, Xie S-P, Primeau F, McWilliams JC, Pasquero C (2015) Northwestern Pacific typhoon intensity controlled by changes in ocean temperatures. Sci Adv 1:e1500014

Mendelsohn R, Emanuel K, Chonabayashi S, Bakkensen L (2012) The impact of climate change on global tropical cyclone damage. Nat Clim Change 2:205–209

Nakagawa T, Okuda M, Yonenobu H, Miyoshi N, Fujiki T, Gotanda K, Tarasov PE, Morita Y, Takemura K, Horie S (2008) Regulation of the monsoon climate by two different orbital rhythms and forcing mechanisms. Geology 36:491–494

Pape JR, Banner JL, Mack LE, Musgrove M, Guilfoyle A (2010) Controls on oxygen isotope variability in precipitation and cave drip waters, central Texas, USA. J Hydrol 385:203–215

Pausata FSR, Battisti DS, Nisancioglu KH, Bitz CM (2011) Chinese stalagmite $\delta^{18}O$ controlled by changes in the Indian monsoon during a simulated Heinrich event. Nat Geosci 4:474–480

Porter SC, An Z (1995) Correlation between climate events in the North Atlantic and China during the last glaciation. Nature 375:305–308

Ren F, Gleason B, Easterling D (2002) Typhoon impacts on China's precipitation during 1957–1996. Adv Atmos Sci 19:943–952

Ruddiman WF (2003) Orbital insolation, ice volume, and greenhouse gases. Quat Sci Rev 22:1597–1629

Ruddiman WF (2006) What is the timing of orbital-scale monsoon changes? Quat Sci Rev 25:657–658

Ruddiman WF (2008) Earth's climate: past and future. W. H. Freeman and Company, New York

Ruddiman WF, Raymo ME (2003) A methane-based time scale for Vostok ice. Quat Sci Rev 22:141–155

Shen Q, Zhang S, Zhao J, Wang X (2013) Contribution of typhoon over coastal waters to summer rainfall in eastern China. Acta Phys Sin 62:189201

Stowasser M, Wang Y, Hamilton K (2007) Tropical cyclone changes in the western North Pacific in a global warming scenario. J Clim 20:2378–2396

Su Q, Peng C, Yi L, Huang H, Liu Y, Xu X, Chen G, Yu H (2016) An improved method of sediment grain size trend analysis in the Xiaoqinghe Estuary, southwestern Laizhou Bay, China. Environ Earth Sci 75:1–10

Sun Y, Clemens SC, An Z, Yu Z (2006) Astronomical timescale and palaeoclimatic implication of stacked 3.6-Myr monsoon records from the Chinese Loess Plateau. Quat Sci Rev 25:33–48

Sun L, Ai W, Song W, Wang Y (2010) Study on climatological characteristics of China-influencing tropical cyclones. J Trop Meteorol 26:60–64

Sun X, Wang X, Zhai S, Lei G, Jiang X (2016) The analysis of the characteristics and water vapor source of the $\delta^{18}O$ in the precipitation of typhoon "Matmo" at Fuzhou. J Nat Resour 31:1041–1050

Thomas EK, Clemens SC, Sun Y, Prell WL, Huang Y, Gao L, Loomis S, Chen G, Liu Z (2016) Heterodynes dominate precipitation isotopes in the East Asian monsoon region, reflecting interaction of multiple climate factors. Earth Planet Sci Lett 455:196–206

Tian J, Zhao Q, Wang P, Li Q, Cheng X (2008) Astronomically modulated Neogene sediment records from the South China Sea. Paleoceanography 23:PA3210

Tu J-Y, Chou C, Chu P-S (2009) The abrupt shift of typhoon activity in the vicinity of Taiwan and Its association with Western North Pacific–East Asian climate change. J Clim 22:3617–3628

Wada A, Usui N (2007) Importance of tropical cyclone heat potential for tropical cyclone intensity and intensification in the Western North Pacific. J Oceanogr 63:427–447

Wada A, Usui N, Sato K (2012) Relationship of maximum tropical cyclone intensity to sea surface temperature and tropical cyclone heat potential in the North Pacific Ocean. J Geophys Res 117:D11118

Wallace JM, Hobb PV (1977) Atmospheric science: an introductory survey. Academic Press, New York

Wang B (1994) Climatic regimes of tropical convection and rainfall. J Clim 7:1109–1118

Wang P (1999) Response of Western Pacific marginal seas to glacial cycles: paleoceanographic and sedimentological features. Mar Geol 156:5–39

Wang B (2006) The Asian monsoon. Springer-Praxis Publishing, Chichester

Wang P (2009) Global monsoon in a geological perspective. Chin Sci Bull 54:1113–1136

Wang B, Ding Q (2008) Global monsoon: Dominant mode of annual variation in the tropics. Dyn Atmos Oceans 44:165–183

Wang P, Prell WL, Blum P (2000) In: Proceedings of the Ocean Drilling Program Initial Reports Volume Leg 184. Texas A&M University, USA

Wang YJ, Cheng H, Edwards RL, An Z, Wu J, Chen C-C, Dorale JA (2001) A high-resolution absolute-dated late pleistocene monsoon record from hulu cave, China. Science 294:2345–2348

Wang YJ, Cheng H, Edwards RL, He Y, Kong X, An Z, Wu J, Kelly MJ, Dykoski CA, Li X (2005) The Holocene Asian monsoon: links to solar changes and North Atlantic climate. Science 308:854–857

Wang JB, Qian W, Zhang X (2007) Relationship between the tropical cyclone genesis over the Northwest Pacific and the sea surface temperature anomalies. Prog Nat Sci 17:1208–1212

Wang YJ, Cheng H, Edwards RL, Kong X, Shao X, Chen S, Wu J, Jiang X, Wang X, An Z (2008a) Millennial- and orbital-scale changes in the East Asian monsoon over the past 224,000 years. Nature 451:1090–1093

Wang YM, Ren F, Li W, Wang X (2008b) Climatic characteristics of typhoon precipitation over China. J Trop Meteorol 24:233–2238

Wang P, Wang B, Cheng H, Fasullo J, Guo Z, Kiefer T, Liu Z (2014) The global monsoon across timescales: coherent variability of regional monsoons. Clim Past 10:2007–2052

Webster PJ, Magaña VO, Palmer TN, Shukla J, Tomas RA, Yanai M, Yasunari T (1998) Monsoons: processes, predictability, and the prospects for prediction. J Geophys Res 103:14451–14510

Webster PJ, Holland GJ, Curry JA, Chang HR (2005) Changes in tropical cyclone number, duration, and intensity in a warming environment. Science 309:1844–1846

Whitney LD, Hobgood JS (1997) The relationship between sea surface temperatures and maximum intensities of tropical cyclones in the Eastern North Pacific Ocean. J Clim 10:2921–2930

Yancheva G, Nowaczyk NR, Mingram J, Dulski P, Schettler G, Negendank JFW, Liu J, Sigman DM, Peterson LC, Haug GH (2007) Influence of the intertropical convergence zone on the East Asian monsoon. Nature 445:74–77

Yang S, Ding Z, Li Y, Wang X, Jiang W, Huang X (2015) Warming-induced northwestward migration of the East Asian monsoon rain belt from the Last Glacial Maximum to the mid-Holocene. Proc Natl Acad Sci USA 112:13178–13183

Yao L, Ren J, Luo Z (2009) Preliminary study on variations of landfalling tropical cyclone rainfall over east China. J Nanjing Inst Meteorol 32:87–93

Yi L, Yu H, Ortiz JD, Xu X, Chen S, Ge J, Hao Q, Yao J, Shi X, Peng S (2012) Late Quaternary linkage of sedimentary records to three astronomical rhythms and the Asian monsoon, inferred from a coastal borehole in the south Bohai Sea, China. Palaeogeogr Palaeoclimatol Palaeoecol 329–330:101–117

Yi L, Ye X, Chen J, Li Y, Long H, Wang X, Du J, Zhao S, Deng C (2014) Magnetostratigraphy and luminescence dating on a sedimentary sequence from northern East China Sea: constraints on evolutionary history of eastern marginal seas of China since the Early Pleistocene. Quat Int 349:316–326

Yi L, Deng C, Xu X, Yu H, Qiang X, Jiang X, Chen Y, Su Q, Chen G, Li P, Ge J, Li Y (2015) Paleo-megalake termination in the Quaternary: paleomagnetic and water-level evidence from south Bohai Sea, China. Sediment Geol 319:1–12

Yi L, Deng C, Tian L, Xu X, Jiang X, Qiang X, Qin H, Ge J, Chen G, Su Q, Chen Y, Shi X, Xie Q, Yu H, Zhu R (2016) Plio-Pleistocene evolution of Bohai Basin (East Asia): demise of Bohai Paleolake and transition to marine environment. Sci Rep 6:29403

Yuan D, Cheng H, Edwards RL, Dykoski CA, Kelly MJ, Zhang M, Qing J, Lin Y, Wang Y, Wu J, Dorale JA, An Z, Cai Y (2004) Timing, duration, and transitions of the last interglacial Asian monsoon. Science 304:575–578

Yue Q, Dong X, Ma K (2000) Climatic characteristics of northwestern Pacific typhoon activity and Chinese coastal landfall typhoon rain and gale. J Nanjing Univ (Natural Sciences) 36:741–749

Zachos J, Pagani M, Sloan L, Thomas E, Billups K (2001) Trends, rhythms, and aberrations in global climate 65 Ma to present. Science 292:686–693

Zhang P, Cheng H, Edwards RL, Chen F, Wang Y, Yang X, Liu J, Tan M, Wang X, Liu J, An C, Dai Z, Zhou J, Zhang D, Jia J, Jin L, Johnson KR (2008) A test of climate, sun, and culture relationships from an 1810-year Chinese cave record. Science 320:940–942

Zhang L, Chen L, Liu J, Liu F, Chen Z (2009) D and $\delta^{18}O$ isotopes in atmospheric precipitation in Hongkong Area. Ecol Environ Sci 18:572–577